Asian Journal of Chemistry; Vol. 36, No. 12 (2024), 2899-2904

ASIAN JOURNAL OF CHEMISTRY

https://doi.org/10.14233/ajchem.2024.32731

Structural, Optical and Hardness Features of Copper Sulphate Crystallites for Optical Applications

HELEN MERINA ALBERT[1,*], T. RAJANI[2], D. NEELIMA PATNAIK[3], M.V. SOMESWARARAO[4], P. VIMALA[5], SANTOSH KUMAR NATHSHARMA[6] and NELLORE MANOJ KUMAR[7]

[1]Department of Physics, Sathyabama Institute of Science & Technology, Chennai-600119, India
[2]Department of Physics, VNR Vignana Jyothi Institute of Engineering and Technology, Hyderabad-500090, India
[3]Department of H&S (Physics), CMR College of Engineering & Technology, Hyderabad-501401, India
[4]Department of Engineering Physics, S.R.K.R. Engineering College, Bhimavaram-534204, India
[5]Department of Chemistry, Muthurangam Government Arts College, Vellore-632002, India
[6]Department of Chemistry, Stewart Science College, Cuttack-753001, India
[7]Department of Mathematics, Saveetha School of Engineering, Saveetha Institute of Medical and Technical Sciences (SIMATS), Thandalam, Chennai-602105, India

*Corresponding author: E-mail: drhelenphy@gmail.com

Received: 19 September 2024; *Accepted*: 8 November 2024; *Published online*: 30 November 2024; AJC-21833

In this investigation, copper sulphate crystals ($CuSO_4$) were produced by a slow evaporation process. Powder-Xay diffraction (PXRD), Fourier transform infrared (FTIR) spectroscopy, UV-visible spectroscopy (UV-vis), second harmonic generation (SHG) and microhardness analyses were used to describe the structural aspects, optical parameters and hardness features of the derived crystals. The XRD measurements show that the $CuSO_4$ crystallized into a triclinic structure and the FTIR method was applied to assess the atomic vibrations in the $CuSO_4$ sample. The UV-Vis measurements demonstrated high transparency of $CuSO_4$ in the near-UV and visible spectra. The optical attributes, including refractive index, extinction coefficient, dielectric constants and optical and electrical conductivities of $CuSO_4$ were determined. The SHG ability of the powdered sample was explored by the Kurtz and Perry method and found to be 1.10 times that of the KDP. The mechanical characteristics of the $CuSO_4$ samples were demonstrated by the Vickers microhardness study. Excellent optical attributes, combined with suitable SHG and mechanical characteristics make the $CuSO_4$ crystals suitable for optoelectronic applications.

Keywords: $CuSO_4$, X-ray diffraction, Second-harmonic generation, Microhardness.

INTRODUCTION

The non-linear optical materials have become increasingly important in science and technology in recent years. Non-linear optics involve non-linear interactions between the light and the medium. The crystals with non-linear optical properties are used for applications including, optical data storage, high-speed communications, frequency shifting, optoelectronics, photonics, *etc*. [1-4]. Pure inorganic crystals are highly advantageous for the impromptu and fast development of rapid optical communication networks. The advancement of existing photonic technologies, such as frequency conversion, optoelectronics, storing data, optical switching, UV filters, optical modulation and detection devices, is a continuous endeavour for the photonic industry's developers. NLO device design is currently greatly aided by the wide range of inorganic compounds, *e.g*. potassium dihydrogen phosphate (KDP), potassium dideuterium phosphate (DKDP), ammonium dihydrogen phosphate (ADP), potassium niobate ($KNbO_3$), lithium niobate ($LiNbO_3$), *etc.* which are the building blocks of photonic devices [5,6]. Transparency, adequate quadratic susceptibility and the thermal stability to withstand powerful lasers without experiencing any negative effects are all necessary for crystals to be of such immense utility. When it comes to creating new NLO crystals, inorganic elements have long been considered the most important component.

The ability of an inorganic class of materials to organize themselves into single crystals that offer wide optical transparency, frequency conversion, better optical response and diele-

ctric features has drawn the attention of researchers [7,8]. The inorganic materials are more advantageous than the organic counterparts in design flexibility and strong mechanical and thermal stability in high-power laser applications.

Researchers must thoroughly examine the intriguing inorganic copper sulphate ($CuSO_4$) crystal. $CuSO_4$ finds important uses in the printing and building sectors, moreover, $CuSO_4$ is used in the artwork and fireworks engineering as a colouring agent. The aqueous solution of $CuSO_4$ is widely used as a resistive element in the electronic liquid resistors [9,10]. Initially, Manomenova *et al.* [11] described the crystal formation of $CuSO_4{\cdot}5H_2O$, suitable for broadband optical filters. However, Justel *et al.* [12] reported the crystallization of $CuSO_4{\cdot}5H_2O$ from a aqueous solution using NaCl. Inspired by the earlier work on $CuSO_4$ crystals, the high-quality $CuSO_4$ crystals were developed by a gradual evaporation procedure in the present study for the optical and nonlinear optical applications.

EXPERIMENTAL

The starting reagent copper sulphate pentahydrate (AR grade) was purchased from Sd-fine Chemicals, India and purified by repeated recrystallization processes to ensure their purity. Recrystallized chemicals were used for the synthesis process. A gradual evaporation process was applied for the formation of $CuSO_4$ crystals. Initially, a saturated solution of $CuSO_4{\cdot}5H_2O$ was prepared using 25 mL of deionized water at 32 ºC. The saturated solution was stirred well for around 4 h by a magnetic stirrer and then filtered using micro-filter paper to remove any remaining contaminants. The solution was subsequently maintained in a 100 mL beaker equipped with a porous cover to promote the gradual evaporation of the solvent. A high-quality $CuSO_4$ crystals with optimum size were obtained in 20 days (Fig. 1).

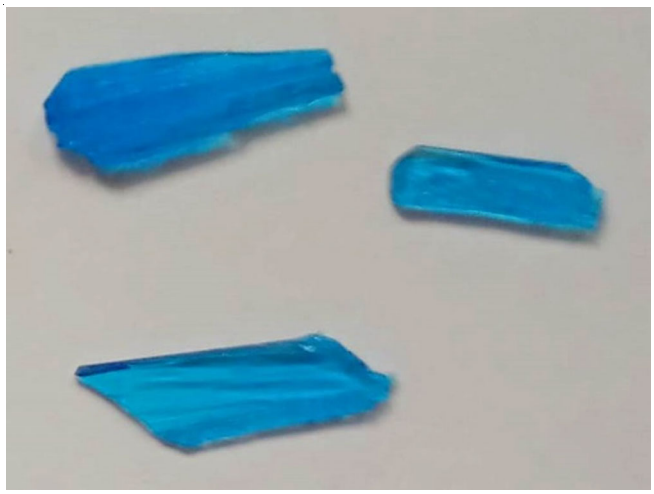

Fig. 1. Photograph of as-produced $CuSO_4$ crystals

Characterization: The detection method includes the structural and physico-chemical characteristic analysis. The Reich-Seifert 3003-TT diffractometer was employed for the powder XRD investigations to investigate the crystal form and lattice constants for the $CuSO_4$ samples. An FT/IR-6600 type-A spectrometer was used to get the FTIR spectrum of the test sample. The optical properties were studied in the UV-visible spectral area using a Jasco International Co., Ltd. (V670 spectrophotometer), Japan. The Kurtz and Perry method was followed to evaluate the second harmonic generation of $CuSO_4$ powdery samples. A temperature-controlled, angle-tuned and extremely effective generator was used for the Kurtz and Perry analysis. The Vickers microhardness machine and a diamond pyramidal indenter were used to measure the hardness nature of the prepared crystals.

RESULTS AND DISCUSSION

P-XRD studies: The most popular non-destructive testing method for identifying crystalline materials is X-ray diffraction (XRD). Tiny $CuSO_4$ samples were chosen for the experimental analysis. The peak intensities were found by scanning the $CuSO_4$ sample in 2θ orientations between 0º and 110º. Fig. 2 shows the XRD peaks of $CuSO_4$ crystal. The diffractogram shows the peaks with 2θ values of 18.964º, 22.48º, 27.68º, 31.84º, 37.72º, 42.50º, 56.97º, 67.75º and 86.62º. A significant peak is found around 18.964º. The crystallographic planes associated with the indexed peaks are (100), (110), (111), (200), (210), (211), (311), (40$\bar{1}$) and (422). Considering the XRD findings, the $CuSO_4$ crystallized in a triclinic configuration with the *P*1 group. The lattice parameters were obtained to be $a = 5.97$Å, $b = 6.11$ Å, $c = 10.70$ Å, $\alpha = 77.27º$, $\beta = 82.32º$, $\gamma = 72.56º$. The values agree rather well with the previously reported data of $CuSO_4$ crystal [13].

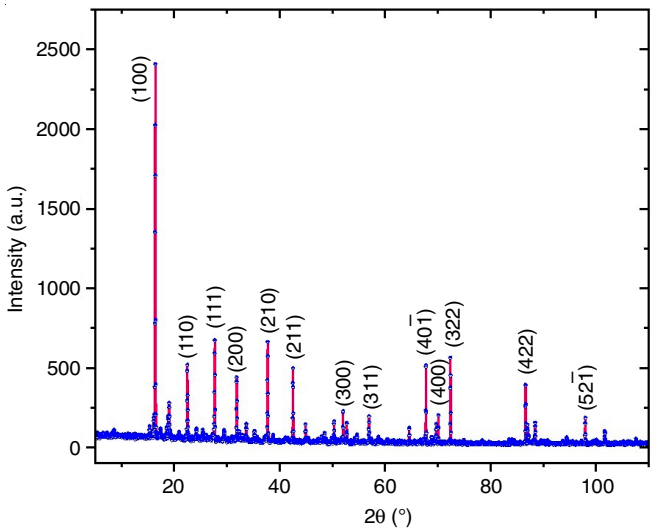

Fig. 2. The XRD spectrum for $CuSO_4$ crystal

FTIR studies: Fig. 3 displays the recorded FTIR spectrum of $CuSO_4$ between 4000 and 400 cm^{-1}. The spectrum shows a broad absorbance band in the higher wavenumber region between 3065 and 3575 cm^{-1}. This broad absorbance is because of the stretching vibration of the water molecules. The weak bands found between 2500 and 2000 cm^{-1} are due to the OH group in the crystal. The strong band at 1623 cm^{-1} is due to the bending mode of the OH group, whereas the strong bands at 1149 and 1091 cm^{-1} are due to the asymmetric and symmetric

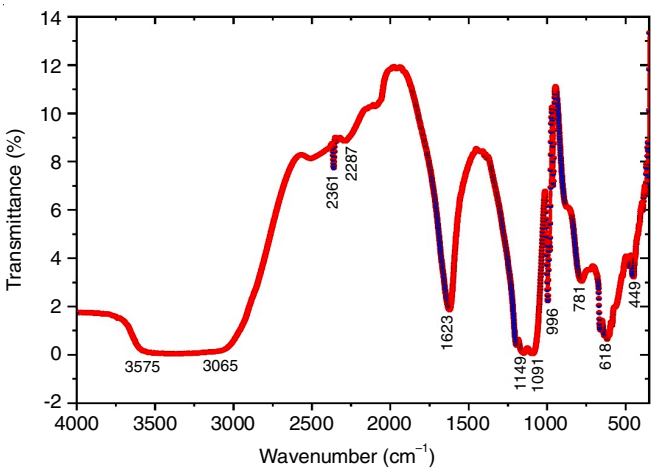

Fig. 3. FT-IR spectrum of $CuSO_4$ crystal

vibrations of the S=O group. The bands at 996 and 618 cm^{-1} are due to the SO_4^{2-} non-degenerate and degenerate modes. The band at 781 cm^{-1} is because of the Cu-O-H coordination, while the peak at 449 cm^{-1} is due to the SO_4^{2-} bending mode.

UV-Vis spectral studies: The optical property was investigated in the 300-650 nm wavelength range and the spectrum (Fig. 4) shows that the transmittance of $CuSO_4$ initially increases from 300 nm and attains a maximum percentage at 325 nm. From 325 nm to 575 nm, the sample shows a constant maximum transmittance and then shows a slight decrease in the transmittance. The $CuSO_4$ sample is highly transparent in the wavelength range between 325 nm and 575 nm, making it suitable for optical applications such as optical bandpass filters in this spectral region. The UV data was interpreted to investigate the optical bandgap of $CuSO_4$. The Tauc formula was applied to determine the absorption coefficient (α) of $CuSO_4$ sample [14]:

$$\alpha h\nu = A(h\nu - E_g)^n$$

where E_g denotes the bandgap; A is the constant and n refers to an integer. For a permissible direct transition, n should be 2. The curve generated between hν and $(\alpha h\nu)^2$ is illustrated in Fig. 5 and based on the plot, the bandgap of $CuSO_4$ is found to be 3.9 eV.

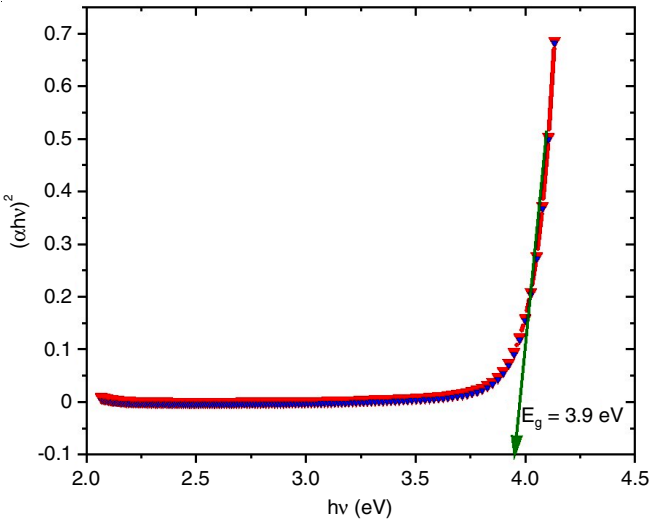

Fig. 5. Tauc plot of prepared CuSO4 crystal

When incident light interacts with a material, it can either be refracted or absorbed; the degree of this relies on the conductivity, refractive index and extinction coefficient of the material [15]. The refractive index (n) was obtained through the following expression:

$$n = \frac{1}{T_S} + \sqrt{\frac{1}{T_S - 1}}$$

where T_S denotes the (%) transmittance.

The wavelength-related variation in the refractive index is displayed in Fig. 6. The curve demonstrates that the refractive index decreases significantly from the 300 to 325 nm range. The refractive index exhibits a slight decrease thereafter, attaining a minimum value of 1.112 within the 350-550 nm wavelength range. With the further wavelength increase, the refractive index marginally increases.

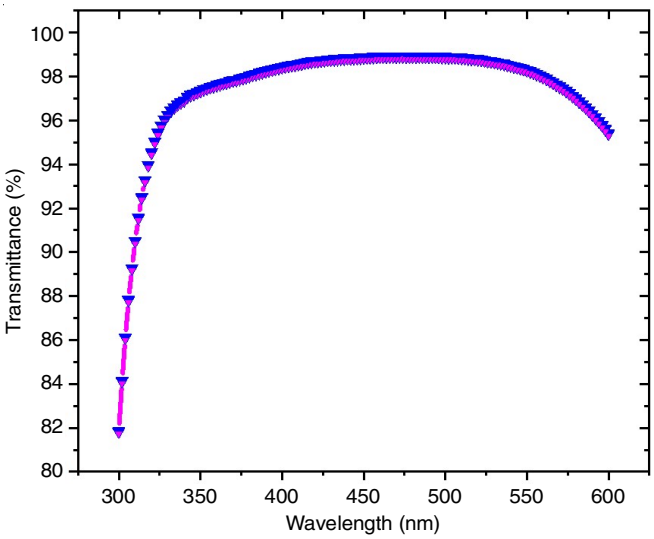

Fig. 4. Optical transmittance spectrum of $CuSO_4$ crystals

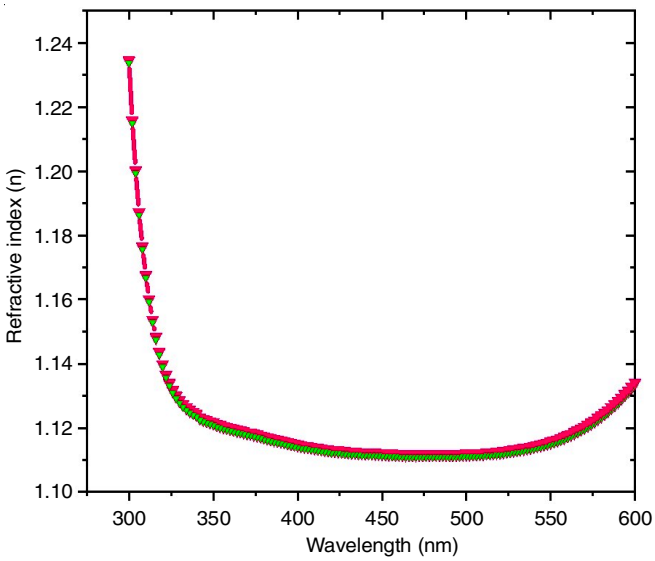

Fig. 6. Plot of variation in the refractive index against wavelength

The potential of an element to either reflect or absorb light at a designated wavelength is represented by its extinction coefficient (k), which can be represented as [16]:

$$k = \frac{\alpha\lambda}{4\pi}$$

Fig. 7 illustrates the correlation between k and λ of light. The curve shows that the k value is maximum at 300 nm. With the increase in wavelength, the k value drecreases considerably, attaining a low value at 325 nm. The k value is the minimum in the 325–550 nm wavelength range. The optical conductance of $CuSO_4$ was evaluated using the below formula [17]:

$$\sigma_{opt} = \frac{n\alpha c}{4\pi}$$

where c is the velocity of light.

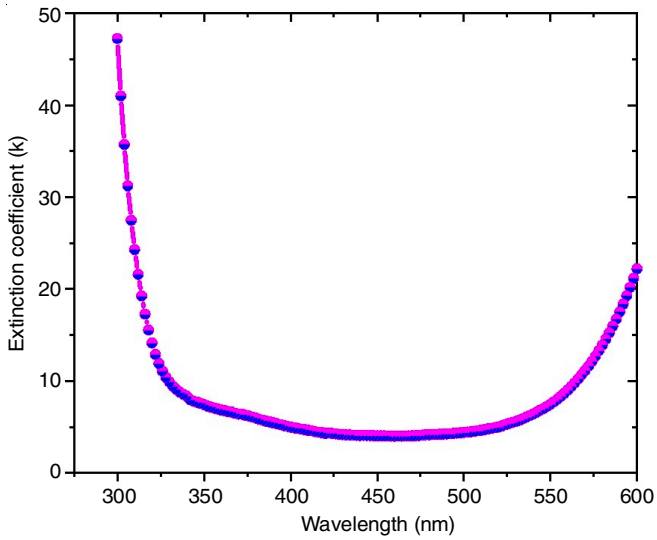

Fig. 7. Plot of extinction coefficient variations with wavelength

Fig. 8 illustrates the dependency of the optical conductance of $CuSO_4$ with the light energy. The optical conductance slightly decreases in the 2.0-2.5 eV energy range and attains a minimal value. After that, the optical conductance slightly increases in the 2.5-3.55 eV energy range, then it increases sharply to reach its maximum at 4.10 eV. The excellent optical conductivity of the prepared $CuSO_4$ crystal validates the remarkable photoresponse of the material. This characteristic improves the suitability of the material for applications involving information processing.

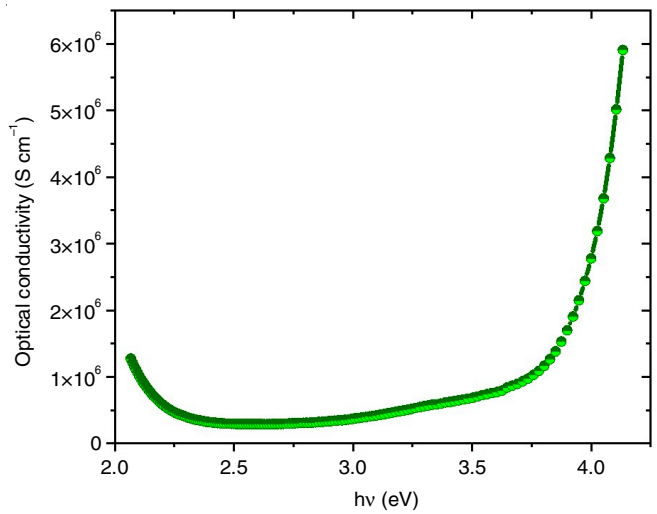

Fig. 8. Plot of variations in optical conductivity against photon energy

The relationship between the electrical conductivity (σ_{ele}), optical conductivity (σ_{opt}) and absorption coefficient (α) is given by the following expression [18]:

$$\sigma_{ele} = \frac{2\lambda\sigma_{opt}}{\alpha}$$

Fig. 9 shows the electrical conductivity variation about the photon energy. The $CuSO_4$ crystal is found to have higher electrical conductivity at the lower energy photons. With the increase in photon energy, the electrical conductivity decreases linearly and attains a minimum value at higher energy.

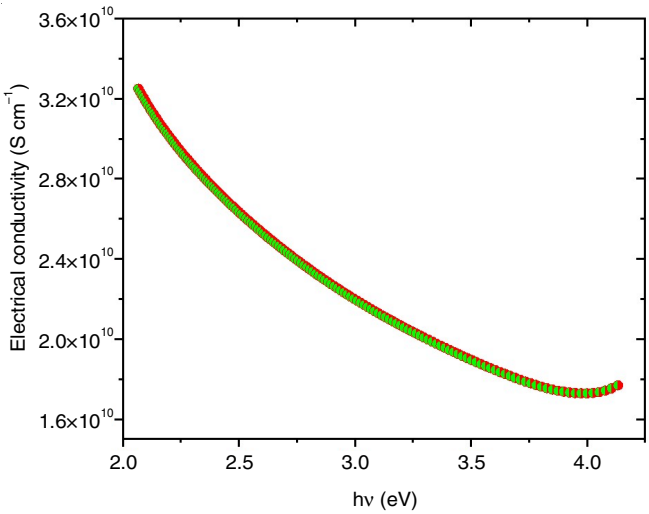

Fig. 9. Plot of variations in electrical conductivity against photon energy

The complex dielectric constant (ε^*) is described by the relation [19]:

$$\varepsilon^* = \varepsilon_1 + i\varepsilon_2$$

The dielectric real (ε_1) and imaginary (ε_2) portions were determined from the relations:

$$\varepsilon_1 = n^2 - k^2 \text{ and } \varepsilon_2 = 2nk$$

Fig. 10 shows the variation of dielectric constant portions ε_1 and ε_2 related to the wavelength. Observations revealed that the real portion (ε_1) behaves like the transmittance spectra, increasing from 300 to 325 nm and then reaching a maximum saturation in the higher wavelength region. On the other hand, the imaginary portion (ε_2) exhibits a steep decline from 300 to 325 nm and then reaches the minimum saturation in the higher wavelength region.

Second harmonic generation test: The SHG value of $CuSO_4$ sample was evaluated with the Kurtz & Perry method [20]. The SHG experiment used a "Q-switched Nd: YAG laser" functioning at 1064 nm with a 6 ns pulse width. The greenish light of $CuSO_4$ powder (532 nm) emission verified the production of the second harmonic radiation. The powdered KDP was

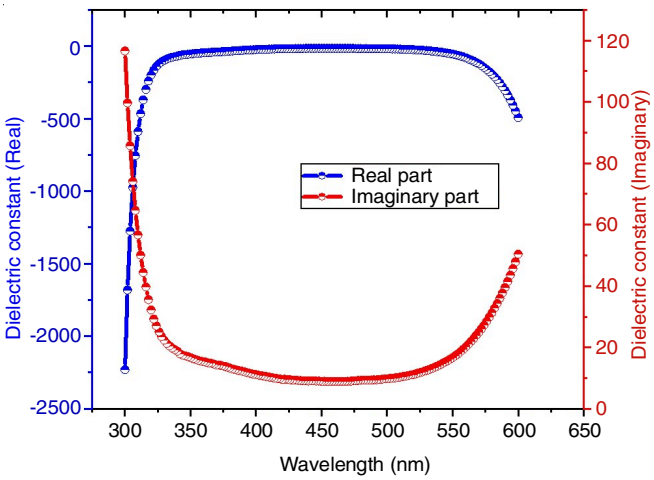

Fig. 10. Variation of the dielectric constants with wavelength

served as the reference material. The prepared $CuSO_4$ was found to have a second harmonic ability 1.10 times that of the KDP.

Microhardness analysis: Hardness measurement is a helpful non-destructive testing technique to ascertain a strength or abilityof the material to withstand deformations [21]. Several features like lattice energy, interatomic spacing, temperature and heat generation affect a material's hardness. The crystalline samples were carefully polished during the experimental procedure to prevent surface imperfections. Loads of varying scales (10, 20, 30, 40 and 50 g) were applied to $CuSO_4$ crystals on the microhardness tester platform for a predetermined time (10 s). Due to the creation of microcracks at greater stresses, the highest applied load was limited to 50 g. The microhardness of $CuSO_4$ was evaluated using the following equation [22]:

$$H_v = \frac{1.8544P}{d^2} Kg/mm^2$$

where, P represents the applied load and d is the typical indentations. The microhardness number (H_v) is shown against the applied load in Fig. 11 and it is observed that the H_v starts at 5 g and increases with increasing load. The graph of Log P *vs.* log d is displayed in Fig. 12. The plot indicates a linear increase in log d with log P. The least-square fit approach was applied to

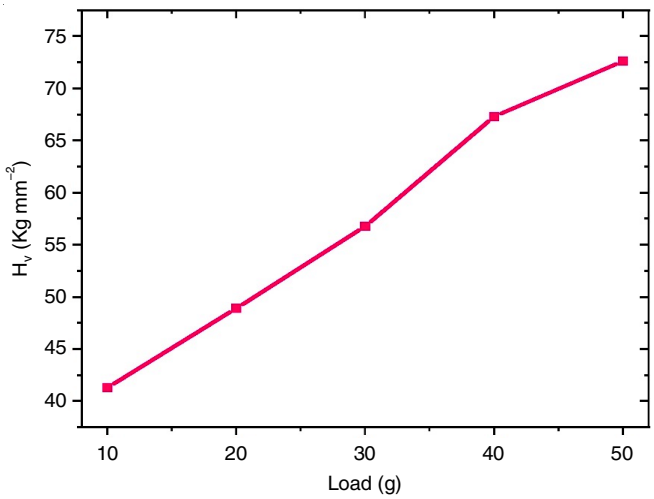

Fig. 11. Variation in the microhardness value (H_v) under applied load (P)

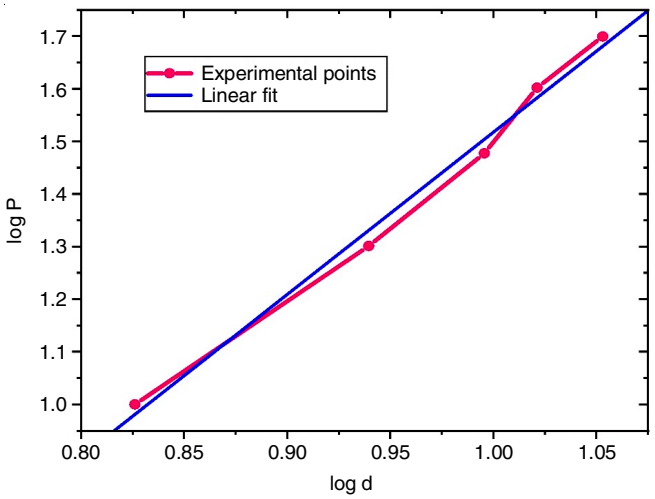

Fig. 12. Variation of log P with log d for crystal$CuSO_4$ crystal

determine the work hardening coefficient (n). According to the Onitsch's proposal, a material is classified as soft if its n value is greater than 1.6 and as hard if it is between 1.0 and 1.6 [23]. The results reveal that the n value is 3.02, representing that $CuSO_4$ is a soft material.

Conclusion

The copper sulphate $CuSO_4$ crystals were produced using the gradual evaporation procedure and characterized by powder-XRD, FTIR, UV-Vis, SHG and microhardness analyses. The XRD measurements show that the $CuSO_4$ crystallized into the triclinic form. The distinct diffraction peaks in the XRD spectrum define the excellent crystalline state of the samples. The optical measurements demonstrated high transmittance of the $CuSO_4$ in the UV-visible spectrum. The bandgap of $CuSO_4$ is found to be 3.9 eV and also have a second harmonic ability 1.10 times that of the KDP. Microhardness analysis indicates that the hardness number H_v increases with the increasing load. The prepared $CuSO_4$ crystals exhibit remarkable optical transparency and optical properties, along with the appropriate second harmonic generation and microhardness characteristics, rendering them suitable for the optoelectronic applications.

CONFLICT OF INTEREST

The authors declare that there is no conflict of interests regarding the publication of this article.

REFERENCES

1. H.M. Albert, T. Jemima and C.A. Gonsago, *J. Fluoresc.*, **34**, 1057 (2024); https://doi.org/10.1007/s10895-023-03335-8
2. V.V. Atuchin, B.G. Bazarov, T.A. Gavrilova, V.G. Grossman, M.S. Molokeev and Z.G. Bazarova, *J. Alloys Compd.*, **515**, 119 (2012); https://doi.org/10.1016/j.jallcom.2011.11.115
3. Z. Yan, J. Fan, S. Pan and M. Zhang, *Chem. Soc. Rev.*, **53**, 6568 (2024); https://doi.org/10.1039/D3CS01136D
4. H.M. Albert, S.S. Saarwin and C.A. Gonsago, *J. Mater. Sci. Mater. Electron.*, **34**, 1407 (2023); https://doi.org/10.1007/s10854-023-10840-w
5. S.M. Azhar, M. Anis, G. Rabbani, M.D. Shirsat, M.I. Baig, S.S. Hussaini, S. AlFaify and M.A. Khan, *Optik*, **185**, 1247 (2019); https://doi.org/10.1016/j.ijleo.2019.03.041

6. M.I. Baig, M. Anis, H. Algarni, M.D. Shirsat and S.S. Hussaini, *Zhongguo Wuli Xuekan*, **63**, 70 (2020); https://doi.org/10.1016/j.cjph.2019.10.015
7. I.Sh. Steinberg, A.V. Kirpichnikov and V.V. Atuchin, *Opt. Mater.*, **78**, 253 (2018); https://doi.org/10.1016/j.optmat.2017.11.025
8. S. Parola, B. Julián-López, L.D. Carlos and C. Sanchez, *Adv. Funct. Mater.*, **26**, 6506 (2016); https://doi.org/10.1002/adfm.201602730
9. N. Preetha, S.E. Muthu and J. Thirupathy, *J. Mater. Sci. Mater. Electron.*, **34**, 932 (2023); https://doi.org/10.1007/s10854-023-10358-1
10. M. Mallik, S. Monia, M. Gupta, A. Ghosh, M.P. Toppo and H. Roy, *J. Alloys Compd.*, **829**, 154623 (2020); https://doi.org/10.1016/j.jallcom.2020.154623
11. V.L. Manomenova, M.N. Stepnova, V.V. Grebenev, E.B. Rudneva and A.E. Voloshin, *Crystallogr. Rep.*, **58**, 513 (2013); https://doi.org/10.1134/S1063774513030152
12. F.L. Justel, D.M. Camacho, M.E. Taboada and K.J. Roberts, *J. Cryst. Growth*, **525**, 125204 (2019); https://doi.org/10.1016/j.jcrysgro.2019.125204
13. G.E. Bacon and D.H. Titterton, *Z. Kristallogr.*, **141**, 330 (1975); https://doi.org/10.1524/zkri.1975.141.5-6.330
14. H. Merina Albert, T. Lohitha, K. Alagarsamy, C.A. Gonsago and V. Vishwakarma, *Mater. Today Proc.*, **47**, 1030 (2021); https://doi.org/10.1016/j.matpr.2021.06.124
15. R. Sangeetha, V. Charles Vincent, G. Bakiyaraj, K. Kirubavathi and K. Selvaraju, *Res. Opt*, **14**, 100607 (2024); https://doi.org/10.1016/j.rio.2024.100607
16. K. Kumar, V.C. Vincent, G. Bakiyaraj, K. Kirubavathi and K. Selvaraju, *Optik*, **226**, 165738 (2021); https://doi.org/10.1016/j.ijleo.2020.165738
17. S. Kulshrestha and A.K. Shrivastava, *AIP Conf. Proc.*, **2220**, 050010 (2020); https://doi.org/10.1063/5.0002152
18. T. Murugan, K.S. Murugesan and B.M. Boaz, *Indian J. Phys. Proc. Indian Assoc. Cultiv. Sci.*, **96**, 3797 (2022); https://doi.org/10.1007/s12648-022-02335-x
19. A.S. Hassanien and I. Sharma, *Physica B*, **622**, 413330 (2021); https://doi.org/10.1016/j.physb.2021.413330
20. S. Kurtz and T. Perry, *J. Appl. Phys.*, **39**, 3798 (1968); https://doi.org/10.1063/1.1656857
21. T.M. Hamdy, *BMC Oral Health*, **24**, 487 (2024); https://doi.org/10.1186/s12903-024-04261-2
22. H.M. Albert, G. Durgadevi, D. Kanimozhi and C.A. Gonsago, *Appl. Phys., A Mater. Sci. Process.*, **130**, 543 (2024); https://doi.org/10.1007/s00339-024-07707-0
23. R.A. Jothi, R.U. Mullai, S. Gopinath, S. Vetrivel and E. Vinoth, *J. Mater. Sci. Mater. Electron.*, **31**, 791 (2020); https://doi.org/10.1007/s10854-019-02587-0